Journal of Alloys and Compounds 1002 (2024) 175448

Contents lists available at ScienceDirect

Journal of Alloys and Compounds

journal homepage: www.elsevier.com/locate/jalcom

In situ preparation of MOF-74 for compact zincophilic surfaces enhancing the stability of aqueous zinc-ion battery anodes

Da Bi [a], Tiantian Zhao [b], Qingxue Lai [a], Jingxiang Zhao [b], Sergey A. Grigoriev [c,d], Yanyu liang [a,*]

[a] Jiangsu Key Laboratory of Electrochemical Energy Storage Technologies, College of Materials Science and Technology, Nanjing University of Aeronautics and Astronautics., 29 Jiangjun Ave, Nanjing 210016, China
[b] College of Chemistry and Chemical Engineering, Key Laboratory of Photonic and Electronic Bandgap Materials Ministry of Education, Harbin Normal University, Harbin 150025, PR China
[c] National Research University "Moscow Power Engineering Institute", 14 Krasnokazarmennaya St., Moscow 111250, Russia
[d] HySA Infrastructure Center of Competence, Faculty of Engineering, North-West University, Private Bag X6001, Potchefstroom Campus, 2531, South Africa

ARTICLE INFO

Keywords:
Zinc-ion batteries
Zinc anode
MOFs
In situ Raman

ABSTRACT

Zinc-ion batteries (ZIBs), while celebrated for their environmental friendliness, abundant material availability, and inherent safety, face significant challenges that curtail their performance and lifecycle. These challenges include the formation of zinc dendrites, susceptibility to electrolyte corrosion, and the propensity for hydrogen evolution reactions. Addressing these critical issues, our research introduces an innovative surface modification strategy for zinc anode of ZIB with mild electrolyte, by the in-situ synthesis of Metal-Organic Framework (MOF-74) facilitated by the mild acidity of a 2,5-dihydroxyterephthalic acid (DHTA) methanol solution. The zincophilic sites and pore structure introduced by MOF-74 to substantially enhance the surface properties of zinc anodes and accelerate the solvation process, enabling uniform zinc deposition, inhibiting dendrite growth, and significantly bolstering corrosion resistance and electrochemical stability. Combination of physical and electrochemical characterization techniques are employed to validate the successful implementation of MOF-74 on the zinc anode surface and its resultant benefits. When tested in full cell setups with α-MnO_2 as the cathode, the MOF-74 modified zinc anodes displayed exceptional cyclic stability and rate performance, surpassing those of unmodified counterparts. This investigation highlights the potential of MOF materials to address the electrochemical challenges facing zinc anodes, offering a straightforward yet efficacious strategy to enhance the performance and longevity of ZIBs.

1. Introduction

As the global demand for sustainable energy solutions continues to grow, aqueous zinc-ion batteries (AZIBs) have become one of the most closely watched energy storage technologies due to their low cost, environmental friendliness, and high safety characteristics [1–6]. Zinc metal, as the ideal anode material in AZIBs, boasts a high theoretical capacity (820 mAh g^{-1}) and a low redox potential [7,8]. However, the zinc anode faces numerous challenges in practical applications, including the formation of zinc dendrites and hydrogen evolution side reactions, which severely limit the battery's cycle life and performance [2,6].

To address these challenges, the academic and industrial communities have conducted extensive research, focusing on strategies such as anode structure design, electrolyte engineering, functional separator design, and solid electrolyte interphase (SEI) design to improve the performance of zinc metal anodes [9–11]. Among these, surface modification of the zinc anode is considered a direct and effective method. Studies have shown that surface modification of zinc anodes can introduce specific functional groups, providing zincophilic sites that guide zinc deposition and control dendrite growth. For example, Zhou et al. achieved a stable zinc anode by spontaneously constructing a carbonyl-containing layer on the Zn anode. The highly electronegative and nucleophilic carbonyl oxygen endows the anode with strong zincophilicity and excellent dendrite suppression ability, favoring ion transport and effectively homogenizing Zn deposition [12]. Additionally, Cao et al. proposed using trace amounts of glucose additives to provide abundant hydroxyl groups, reshaping the zinc anode surface for

* Corresponding author.
E-mail address: Liangyy403@126.com (Y. liang).

https://doi.org/10.1016/j.jallcom.2024.175448
Received 20 May 2024; Received in revised form 22 June 2024; Accepted 2 July 2024
Available online 3 July 2024

uniform zinc deposition and enabling stable long-term cycling at low temperatures [13].

In addition, by introducing a protective layer on the surface of zinc metal, it is possible to effectively prevent direct contact between the electrolyte and the zinc metal, thereby inhibiting corrosion and hydrogen evolution reactions, and reducing the formation of zinc dendrites [9,14–20]. Metal-organic frameworks (MOFs), with their unique porous structures, high surface areas, and tunable chemical compositions, are considered to have great potential as materials for surface modification of zinc anodes. The zinc anode surface/interface, constructed through the design of components and morphology of MOFs, can effectively block the corrosion of the zinc anode by the electrolyte, as well as promote the uniform transmission and deposition of ions on the zinc anode surface structure, thereby inhibiting the growth of zinc dendrites and improving the cycle stability and performance of the battery [21–26]. However, notwithstanding the considerable potential demonstrated by metal-organic framework (MOF) materials in augmenting the electrochemical attributes of zinc anodes, their deployment is confronted with significant impediments. Zhou et al. coated the zinc anode surface with hydrothermally synthesized ZIF-7 to regulate the solvation structure of the electrolyte. This modification prevents large-radius solvated ions from passing through the MOF micropores, creating a supersaturated electrolyte by removing as many water molecules as possible from the MOF channels. The Zn anode with the ZIF-7 coating exhibits an exceptionally long lifespan and shows uniform zinc deposition with minimal structural changes [21]. Yuan et al. coated the zinc anode surface with zinc benzene tricarboxylate MOF (Zn-BTC-MOF) as a multifunctional protective layer. The Zn-BTC-MOF layer exhibits a uniform microporous three-dimensional channel structure. Additionally, the hydrophilic MOF and the aqueous electrolyte interact more effectively. The Zn-BTC-MOF framework creates a uniform Zn^{2+} flux, thereby promoting homogeneous zinc stripping and plating [27].

Through the aforementioned research, this study explores the introduction of a large number of oxygen-containing functional groups zincophilic sites on the zinc anode surface by MOFs materials. Additionally, the pore structure of MOFs is utilized to improve zinc deposition and accelerate the desolvation process. Most current studies, including those mentioned above, employ a non-in-situ synthesis method, such as doctor-blading, to modify the zinc anode surface with MOFs. This approach often results in poor adhesion and relatively thick MOF layers. Therefore, designing an in-situ synthesized MOF layer presents a superior surface modification strategy for zinc anodes. Moreover, it is crucial to select stable MOF materials tailored to the electrolyte system in use.

By growing MOFs on the surface of zinc metal anodes to introduce zincophilic sites such as -OH and C═O to guide zinc ion deposition while utilizing the pore structure of MOFs to accelerate the desolvation process, the growth of zinc dendrites and hydrogen evolution side reactions can be effectively suppressed. This approach enhances the long-term cycling stability of zinc anodes and zinc-ion batteries. In this study, for the weakly acidic zinc-ion electrolyte system, a stable MOF was selected as the surface modification material for the zinc anode. Utilizing the weak acidity of a 2,5-dihydroxyterephthalic acid (DHTA) methanol solution and the rapid nucleation of MOF-74, a simple and efficient in-situ growth strategy was proposed to achieve MOF-74 surface modification of the zinc metal anode, thereby achieving the aforementioned objectives.

2. Results and discussion

As shown in the Fig. 1, the mild acidity of the DHTA methanol solution slowly corrodes the zinc metal, causing the release of Zn^{2+} from the surface of the zinc foil, which then reacts with DHTA at coordination sites in situ on the zinc foil surface to form MOF-74. The strategy of in-situ synthesizing MOF-74 to modify the zinc anode surface is proposed for the first time in this study. The MOF-74 layer, constructed with homogenous zinc ions, forms a more intimate contact with the zinc anode surface, playing a crucial role in suppressing side reactions and enhancing cycling stability. For the bare zinc anode, once zinc ions begin to deposit and form initial deposition sites on its surface, these protruded

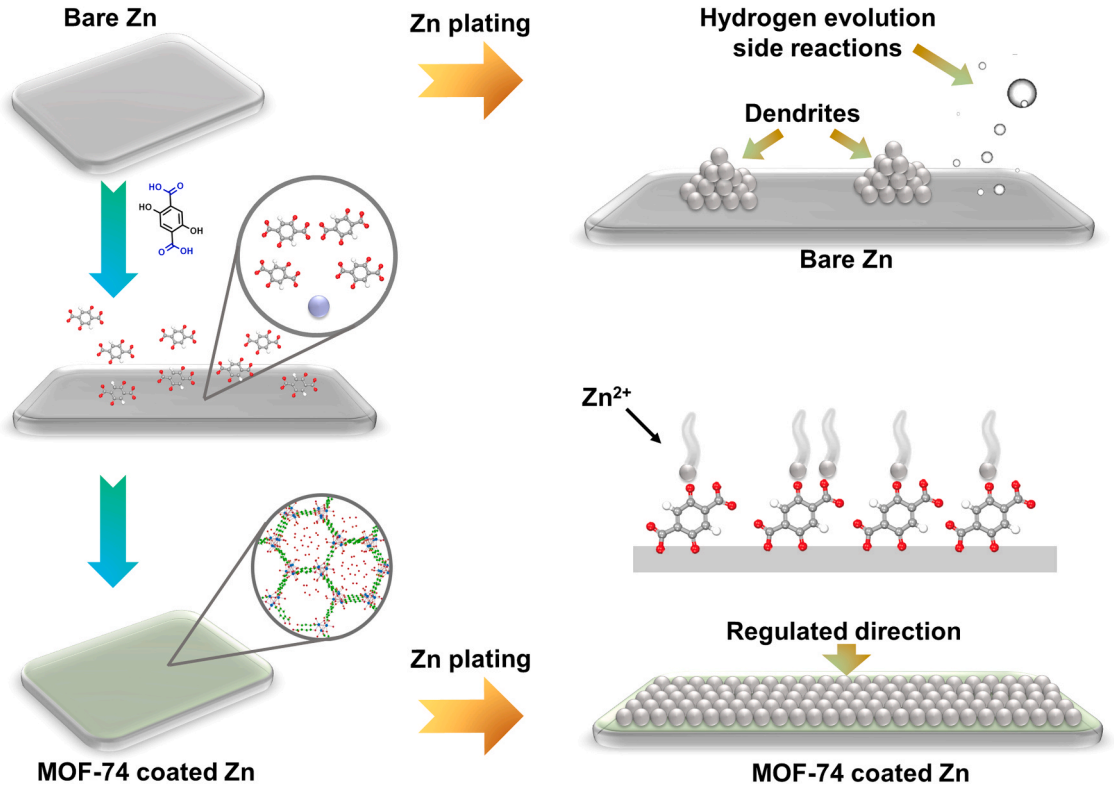

Fig. 1. Synthesis schematic illustration of MOF-74 coated Zn and Zn deposition processes on MOF-74 coated Zn and bare Zn.

surfaces lead to an accumulation of charge, which in turn makes zinc ions more prone to deposit on these protrusions, thereby causing the formation of zinc dendrites. The MOF-74 grown in situ on the zinc foil contains a large number of oxygen-containing functional groups, providing numerous zincophilic sites. When zinc metal modified by the MOF-74 surface serves as the anode for AZBs, these zincophilic sites facilitate zinc nucleation, leading to more uniform zinc deposition on the anode surface and thus inhibiting the growth of zinc dendrites. Moreover, the MOF-74 layer, stable under mild acidic conditions, acts as a physical barrier that effectively prevents chemical corrosion of the zinc anode by the electrolyte. Additionally, the presence of the MOF-74 layer significantly accelerates the desolvation process and increases the hydrogen evolution overpotential of the zinc anode, suppressing the occurrence of hydrogen evolution side reactions.

Scanning Electron Microscopy (SEM) observations revealed that the zinc foil surface treated with DHTA methanol solution was rougher than that of bare zinc (Figure S1, Fig. 2a). Further elemental analysis of the treated zinc foil surface by Energy Dispersive Spectroscopy (EDS) (Fig. 2b) and mapping results showed the presence of carbon (C) and oxygen (O) elements, indicating the successful introduction of ligands on the zinc foil surface. Additionally, the analysis of X-ray Diffraction (XRD) patterns further confirmed the successful synthesis of MOF-74 (Fig. 2c). The treated zinc foil exhibited clear and distinct diffraction peaks at 2Theta positions of 7°, 11.5°, and 17.5°, corresponding to the characteristic peaks of the (110), (300), and (410) crystal planes of MOF-74, respectively [28,29]. These experimental results collectively confirm the successful in situ growth of MOF-74 on the zinc foil surface treated with the DHTA methanol solution. Fourier transform infrared (FTIR) was employed to further characterize the MOF-74 synthesized using this in-situ synthesis method. As shown in Figure S2, the results indicated that the peak at 1639 cm^{-1} corresponds to the presence of carboxyl groups that were not coordinated with zinc ions. The peak at 1558 cm^{-1} was attributed to the successful coordination of the carboxyl groups in the DHTA ligand with zinc ions [30,31]. The peak at 1190 cm^{-1} indicated the presence of C-O single bonds [32]. These results suggested that oxygen-containing functional groups such as C-O and C═O were present on the surface of the zinc anode with in-situ grown MOF-74. Employing the chronopotentiometry to facilitate zinc deposition on the zinc anode surface, at a current density of 2 mA cm^{-2} and a capacity density of 1 mAh cm^{-2}, Scanning Electron Microscopy (SEM) imagery revealed the predominance of clustered zinc formations on the bare zinc surface (Fig. 2d, e). Conversely, the surface of the zinc anode modified with MOF-74 exhibited a homogeneous growth of flake-like metallic zinc. This outcome underscores the significant role of MOF-74 modification in enhancing the uniformity of zinc deposition across the anode surface. Furthermore, optical microscopy (Fig. 2f) provided a macroscopic view revealing the onset of black zinc dendrite formation on the bare zinc surface—an indicator of the non-uniform growth characteristic of metallic zinc during the deposition process. On the contrary, the zinc anode surface modified by MOF-74 displayed a smooth and even appearance, with no discernible dendritic growth. These findings demonstrate that MOF-74 modification facilitates a more uniform zinc deposition on the zinc anode surface, effectively suppressing dendrite formation, and thereby contributing to the improvement of the electrochemical performance and stability of the zinc anode.

Density Functional Theory (DFT) calculations were utilized to study the interactions between MOF-74 and bare zinc with zinc atoms. As illustrated in Fig. 3a, the binding energy between zinc atoms and the zinc (001) crystal surface is −0.44 eV, indicating only weak interactions. In contrast, the interaction between MOF-74 and zinc atoms shows a lower binding energy of −2.84 eV, suggesting a significantly stronger interaction compared to bare zinc [33]. Additionally, the stronger adsorption energy between the zinc anode surface and zinc ions facilitates the desolvation process of zinc ions, inhibiting the hydrogen evolution side reaction [34,35]. The zinc anode uniformly coated with MOF-74 can provide more nucleation sites, leading to the formation of small and dense zinc nuclei and, subsequently, a uniform deposition of zinc. This is beneficial for suppressing dendrite growth caused by nucleation difficulties and the tip effect. During zinc deposition on the zinc anode surface at a current of 1.0 mA cm^{-2}, the nucleation overpotential of the MOF-74 modified zinc anode (29.5 mV) is significantly lower than that of bare zinc (34.6 mV), indicating that nucleation is

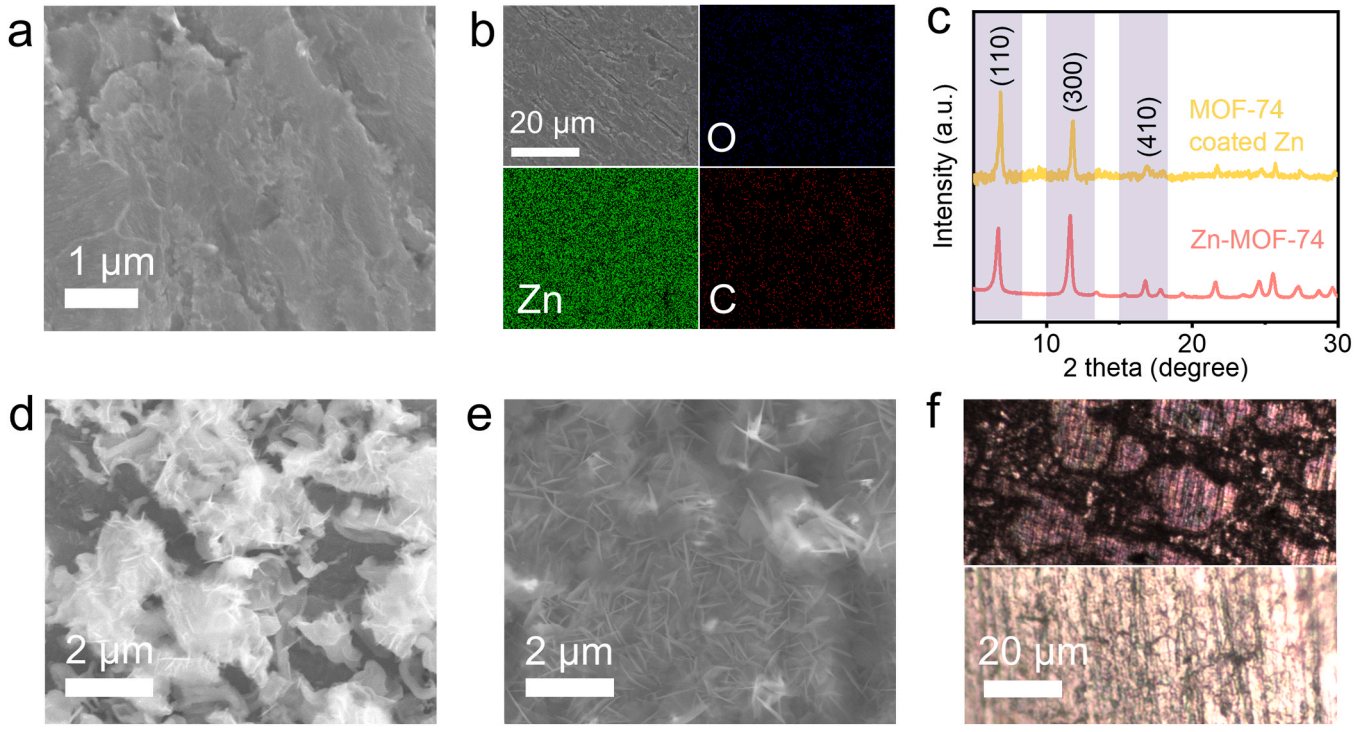

Fig. 2. (a) SEM of the surface of MOF-74 coated Zn. (b) SEM and corresponding mapping. (c) XRD patterns of MOF-74 coated Zn. SEM images of (d) bare Zn and (e) MOF-74 coated Zn after Zn deposition of 1 mAh cm^{-2} and (f) optical picture.

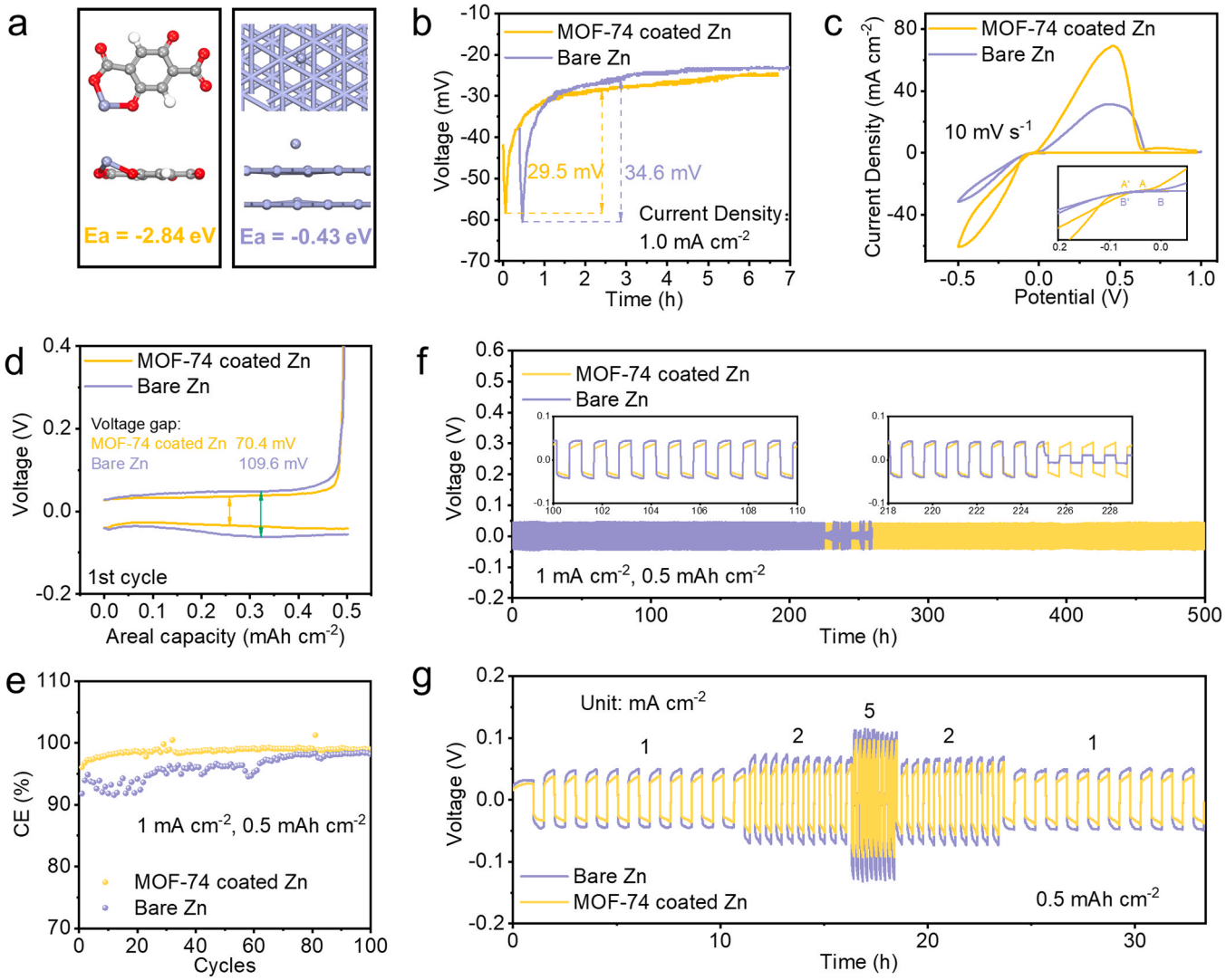

Fig. 3. (a) Binding energy of the Zn atom adsorbed on the MOF-74 coated Zn (left) and bare Zn (right) surfaces. (b) The nucleation overpotentials of Zn electrodeposition. (c) CV curves and partial enlargement (inset) of bare Zn//Cu and MOF-74 coated Zn//Cu cells at 10 mV s^{-1}. (d) The initial discharge/charge voltage gap of Zn//Cu cells and The (e) CE. (f) Cycling performance of the bare Zn and MOF-74 coated Zn symmetric cells at 1 mA cm^{-2}. (g) Rate performance comparison of MOF-74 coated Zn and bare Zn anodes.

easier, which is consistent with theoretical calculations (Fig. 3b). The cyclic voltammetry curve for Zn||Cu further confirms that MOF-74 modification can significantly improve the plating/stripping reaction kinetics of the zinc anode. In the CV curve (Fig. 3c), the nucleation overpotential of the MOF-74 modified zinc anode, denoted as AA', is significantly lower than that of the bare zinc anode, BB'. Moreover, a greater peak current density in the redox peaks of the MOF-74 modified zinc anode implies faster deposition kinetics. Fig. 3d shows the first cycle of constant current charge-discharge for Zn||Cu and MOF-74 coated Zn||Cu batteries, revealing that the MOF-74 modified zinc anode exhibits a lower voltage hysteresis (70.4 mV) compared to the bare zinc electrode battery (109.6 mV), with no significant change in voltage hysteresis after 20 cycles (Figure S3). During the initial 60 cycles, the coulombic efficiency of the bare zinc electrode for the Cu battery is consistently lower than that of the MOF-74 modified zinc anode, indicating that zinc deposition is more uniform on the surface of the modified anode from the start, with fewer by-products formed (Fig. 3d). As shown in Fig. 3e, in the initial 60 cycles, the coulombic efficiency of the bare Zn anode in the Zn-Cu cell was consistently lower than that of the MOF-74 coated Zn anode, indicating that from the beginning, zinc deposition on the modified zinc anode surface was more uniform and produced fewer side reaction byproducts [36,37].

Chronoamperometry test and electrochemical impedance spectroscopy (EIS) before and after chronoamperometry test were employed to determine the Zn^{2+} transfer numbers of bare Zn and MOF-74 coated Zn. The Zn^{2+} transfer numbers were calculated using the following formula [34,38,39]:

$$t_{Zn^{2+}} = \frac{I(\Delta V - I_0 R_0)}{I_0(\Delta V - IR)}$$

I is the polarized equilibrium current, I_0 is the initial current, R is the impedance after polarization equilibrium, R_0 is the initial impedance, and ΔV is the polarization voltage (20 mV). The results are shown in Figure S4. the $t_{Zn^{2+}}$ of MOF-74 coated Zn is 0.52, which is larger than the 0.38 of pure Zn. The results indicate that the MOF-74 layer facilitates the construction of a good solid-liquid reaction interface, enhancing zinc ion conduction. Additionally, as shown in Figure S5, the current density in the chronoamperometry test for MOF-74 coated Zn was significantly higher than that of bare Zn, and the corresponding impedance was significantly lower. The symmetrical cell constructed with MOF-74 coated Zn exhibits significantly higher ionic conductivity compared to bare Zn.

In addition, overcharging tests were conducted on symmetrical cells. As shown in Figure S6, during continuous deposition at a current density of 1 mA cm^{-2}, the MOF-74 coated Zn anode maintained stable zinc deposition for over 90 h, while the bare zinc surface failed rapidly after 18 h. These results suggested that the MOF-74 coated Zn surface provided more nucleation sites, facilitating uniform and stable zinc deposition [38]. Furthermore, the failure process in the bare zinc anode cells was marked by a sharp increase in overpotential, indicating internal disconnection mainly caused by electrolyte depletion and gas generation. This demonstrated that the MOF-74 coated Zn anode significantly inhibited surface side reactions.

Further evaluation was conducted using symmetric cells under constant current charge-discharge at current densities of 2 mA cm^{-2} and 5 mA cm^{-2}, with both charging and discharging times set at 15 min (Figure S7). At a current density of 2 mA cm^{-2}, the bare zinc anode exhibited greater voltage hysteresis and more severe polarization in the initial cycles compared to the MOF-74 modified zinc anode. At a higher current density of 5 mA cm^{-2}, although polarization phenomena were more severe for both the bare and modified anodes than at 2 mA cm^{-2}, the impact was notably more significant on the bare zinc anode, with voltage hysteresis consistently higher than that of the MOF-74 modified zinc anode. In long-cycle tests of symmetric cells (Fig. 3f), constant current charge-discharge was performed at a current density of 1 mA cm^{-2} and a capacity density of 0.5 mAh cm^{-2}. When the bare zinc anode cycled up to 225 h, a sharp voltage drop indicated an internal short circuit within the cell, rendering the battery unable to continue charging or discharging. The short circuit was generally caused by excessive dendrite growth, with dendrites piercing the separator and causing a short circuit between the anode and cathode. Additionally, repeated tests also showed a sudden increase in the charge-discharge voltage of symmetric cells, which could not maintain stable charging or discharging, typically caused by side reactions on the electrode surface leading to hydrogen evolution and electrolyte depletion, resulting in poor solid-liquid interface contact. In contrast, the MOF-74 modified zinc anode's symmetric cell maintained stable charge-discharge cycles for over 500 h without any sudden increase or decrease in voltage, demonstrating significantly enhanced charge-discharge stability over the bare zinc anode's symmetric cell. In the rate performance tests of symmetric cells (Fig. 3g), under the condition of maintaining a charge-discharge capacity density of 0.5 mAh cm^{-2} and varying current densities of 1, 2, and 5 mA cm^{-2}, the MOF-74 modified zinc anode's symmetric cells exhibited lower and more stable overpotentials at all current levels. When the current density was gradually reduced from 5 mA cm^{-2} to 1 mA cm^{-2}, the overpotentials of both the MOF-74 modified and bare zinc anodes recovered well to their initial levels. The reduced overpotential in symmetric cells further clarifies that MOF-74 modification leads to better zinc plating/stripping processes on the zinc anode surface and more stable long-cycle stability. This, in turn, is beneficial for enhancing the overall charge-discharge performance and long-cycle stability of the full cell, promoting the commercial application of rechargeable zinc-ion batteries. Furthermore, high current density and high capacity density charge-discharge tests on the symmetrical cell with the MOF-74 coated Zn anode were conducted, as shown in Figure S8. At a current density of 20 mA cm^{-2} and a capacity of 10 mAh cm^{-2}, the MOF-74 coated Zn symmetrical cell operated stably for over 100 h. This demonstrates the potential application of MOF-74 coated Zn anodes in high current density and high capacity density devices.

To further highlight the role of in-situ synthesis in this study, deposition overpotential at a current density of 2 mA cm^{-2} and the symmetrical cell cycling stability at 1 mA cm^{-2} with a capacity of 0.5 mAh cm^{-2} between zinc anodes synthesized in-situ and ex-situ were compared. As shown in Figure S9, the ex-situ synthesized zinc anode exhibited higher nucleation overpotential (85.9 mV) compared to the in-situ synthesized MOF-74 coated zinc anode (49.0 mV). Additionally, during the symmetrical cell cycling, the ex-situ synthesized zinc anode showed higher voltage hysteresis, which sharply increased after 280 h (Figure S10), leading to cell failure. These electrochemical tests indicated that the ex-situ synthesized MOF-74 coated zinc surface has more difficulty in nucleation, greater polarization, and significantly poorer cycling stability compared to the in-situ synthesized Zn anode.

In situ Raman spectroscopy was utilized to further investigate the zinc deposition process on the surfaces of MOF-74 modified zinc anodes and bare zinc anodes (Fig. 4a). A significant Raman signal was observed at a wavenumber of 465 cm^{-1} for bare zinc, with the signal intensity increasing as deposition proceeded. This Raman signal corresponds to the Zn-OH signal on the anode surface, indicative of zinc corrosion caused by hydrogen evolution and other side reactions. Such corrosion inevitably leads to a gradient in Zn^{2+} concentration and sluggish zinc ion diffusion dynamics, further resulting in uneven zinc deposition. However, no significant signal was observed within the corresponding wavenumber range for the MOF-74 modified zinc anode, indicating that the presence of MOF-74 inhibits corrosion of the zinc anode, effectively protecting it. The Raman signal at 980 cm^{-1} corresponds to SO_4^{2-}, whose presence is related to the concentration of Zn^{2+}. When there is an enrichment of Zn^{2+} on the surface of the zinc anode, influenced by charge balance, the concentration of SO_4^{2-} on its surface also increases accordingly [40,41]. This enrichment of Zn^{2+} is caused by polarization on the anode surface, and when the deposition rate on the anode surface is slow, it leads to an accumulation of Zn^{2+}. The bare zinc surface exhibited a strong signal at 980 cm^{-1} that intensified with ongoing deposition, while the in situ Raman results for the modified zinc anode showed lower signal intensity at the corresponding wavenumber with no significant changes [21,42,43]. After zinc deposition at a current density of 5 mA cm^{-2} for 30 min, a direct visual comparison revealed that the color of bare zinc noticeably darkened, while no significant blackening was observed on the MOF-74 modified zinc anode (Figure S11). These results demonstrate that the introduction of a large number of zincophilic sites through MOF-74 modification significantly enhances zinc deposition, and the corrosion inhibition provided by the MOF-74 modified surface further enhances the reaction dynamics of the deposition process.

As depicted in Fig. 4b, to more intuitively observe the morphological evolution of the zinc anode with zinc deposition, the zinc deposition process on the zinc anode surface under a current of 5 mA cm^{-2} was observed in situ using an optical microscope. When the deposition time reached 20 min, tiny protrusions could be observed on the surface of the bare zinc anode. As time progressed, under the influence of the "tip effect," the uneven deposition became increasingly severe, with these protrusions visibly enlarging. In contrast, the zinc anode modified with MOF-74 maintained a smooth state throughout, and even when the deposition time reached 120 min, corresponding to a deposition capacity of 10 mAh cm^{-2}, the MOF-74 modified zinc anode surface still remained dendrite-free and smooth, whereas the surface of the bare zinc anode had developed a large number of dendrites. This aligns with the results observed in SEM analyses and the outcomes from the long-cycle charge-discharge tests of the symmetric cells.

Electrochemical Impedance Spectroscopy (EIS) test results showed that the interface impedance of the zinc anode modified with MOF-74 was significantly reduced compared to the bare zinc, indicating that the modified zinc anode surface provided a more zincophilic interface and higher charge transfer efficiency (Fig. 5b). Additionally, the corrosion resistance of the zinc anode was studied using Tafel polarization curves. Results in Fig. 4c demonstrate that the MOF-74 modified zinc anode exhibited a more positive corrosion potential and a lower self-corrosion current density (1.49 mA cm^{-2}) compared to 1.97 mA cm^{-2} for the bare zinc anode, indicating that MOF-74 modification reduced the self-corrosion rate of the zinc anode [44]. In the calculation of the electrocatalytic hydrogen evolution ternary diagram (Fig. 4e), materials with higher hydrogen adsorption free energy have lower catalytic activity, i.e., better suppression of hydrogen evolution. The calculation results showed that the hydrogen adsorption free energy of the MOF-74 modified zinc anode was significantly higher than that of the bare zinc

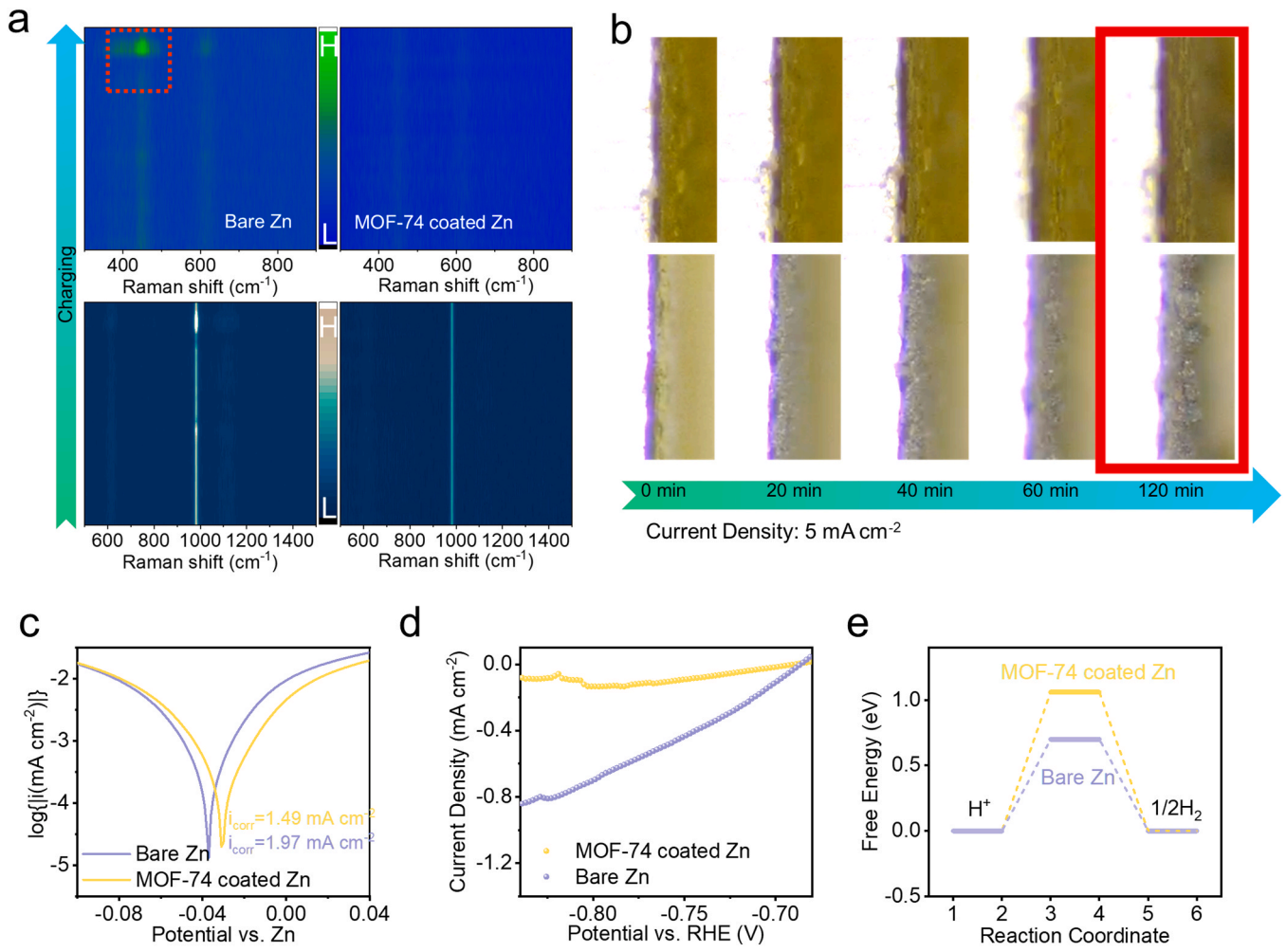

Fig. 4. (a) In situ Raman bare Zn and MOF-74 coated Zn during charging process. (b) In situ optical pictures of Zn deposition after different time. (c) Linear polarization curves of bare Zn and MOF-74 coated Zn. (d) LSV of the both electrodes. (e) Adsorption free energy diagram of the HER.

anode, theoretically proving that MOF-74 modification is beneficial for suppressing the electrochemical hydrogen evolution side reaction. From the LSV curves of the HER reaction (Fig. 4d), it is clear that the electrochemical hydrogen evolution reaction on the MOF-74 modified zinc anode is significantly weaker than on the bare zinc anode (with a lower current density at the same HER potential), indicating that MOF-74 modification suppressed the occurrence of the electrochemical hydrogen evolution side reaction, consistent with theoretical calculation results [45–47].

The modification with MOF-74 significantly improved the zinc deposition and dissolution processes on the zinc anode. Using α-MnO_2 as the cathode material and a weakly acidic zinc sulfate solution as the electrolyte, a full cell was assembled to verify its effectiveness in practical applications of aqueous zinc-ion batteries. As shown in Fig. 5a, redox peaks corresponding to MnO_2 were observed in the cyclic voltammetry (CV) curves of both the MOF-74 modified and bare zinc anode full cells. The MOF-74 modified zinc anode exhibited a more positive reduction peak potential and a more negative oxidation peak potential, indicating a smaller redox overpotential. Additionally, the CV of the full cell with the MOF-74 modified zinc anode displayed a larger peak current density. In the first charge-discharge curve (Fig. 5c), the full cell with the MOF-74 modified zinc anode showed a higher charge-discharge capacity and a smaller voltage hysteresis. In the rate performance tests (Fig. 5d), at various current densities, the full cell with the MOF-74 modified zinc anode demonstrated a higher specific capacity, and when shifting from high to low current densities, it exhibited good capacity recovery, showing overall better rate performance. In the long-cycle charge-discharge tests (Fig. 5d), the full cell with the MOF-74 modified zinc anode displayed a higher initial specific capacity of the positive electrode (208 mAh g^{-1}) and a significantly smaller capacity fade compared to the full cell assembled with a bare zinc anode. After 1000 cycles at a current density of 0.2 A g^{-1}, the positive electrode specific capacity of the MOF-74 modified zinc anode full cell still remained at 161 mAh g^{-1}, with a capacity retention rate of 77.4 %. These performance test results of the Zn-MnO_2 full cell demonstrate that the MOF-74 modified zinc anode provides better plating/stripping surfaces, excellent resistance to hydrogen evolution side reactions, and corrosion resistance. These advantages result in the full cell with the MOF-74 modified zinc anode exhibiting less polarization, better reversibility, and stability.

3. Conclusion

This work introduces an efficient surface modification strategy for zinc anodes in weakly acidic systems. By leveraging the mild acidity of a 2,5-dihydroxyterephthalic acid (DHTA) methanol solution, the zinc anode surface is slowly corroded, facilitating the in-situ formation of MOF-74. The incorporation of MOF-74 provides a multitude of zincophilic sites on the zinc anode, promoting uniform deposition of metallic zinc on the electrode surface, effectively preventing zinc aggregation and dendrite formation. Additionally, the zinc anode modified with MOF-74 exhibits improved corrosion resistance and effective

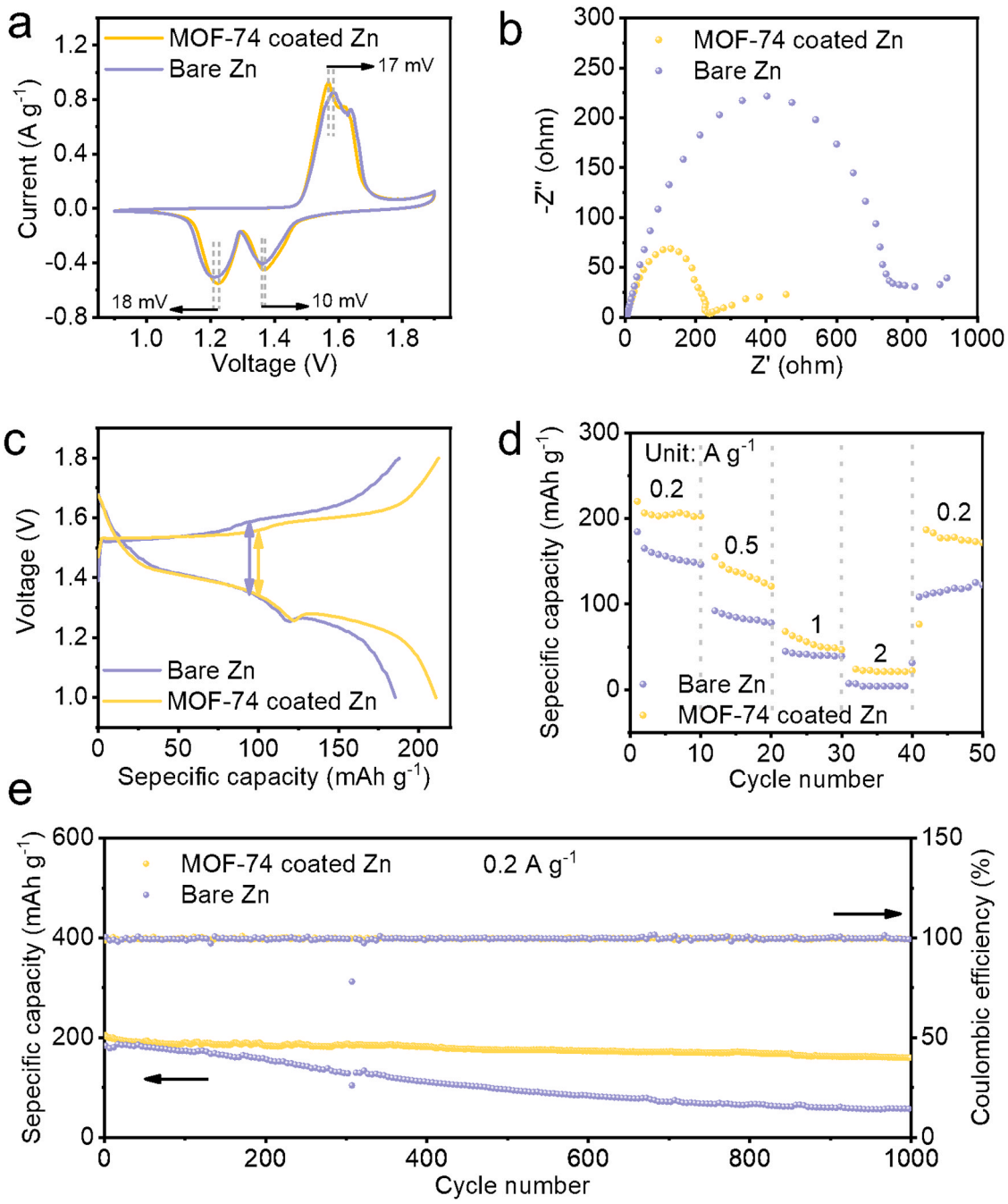

Fig. 5. Comparison of electrochemical performances of Zn//MnO_2 full cells using the MOF-74 coated Zn and bare Zn anodes. (a) CV curves at 0.1 mV s^{-1}. (b) Initial impedance curves. (c) First charge–discharge curves at 0.2 A g^{-1}. (d) Rate performance of bare Zn and MOF-74 coated Zn anodes. (e) Long-term cycling test at 0.2 A g^{-1}.

suppression of electrochemical hydrogen evolution side reactions, further enhancing the electrochemical stability and lifespan of the zinc anode. After modification with MOF-74, the nucleation overpotential of the zinc anode is reduced, and its stability is enhanced. In a full cell with MnO_2 as the cathode, it demonstrates outstanding long-term cycle stability and rate performance. This method of modifying the zinc anode through the in-situ growth of MOF not only is straightforward and efficient but also effectively inhibits the growth of zinc dendrites by introducing a large number of zincophilic sites on the zinc anode surface. This approach offers innovative methodological support for the commercial deployment of zinc-ion batteries (ZIBs) and other energy storage systems utilizing zinc anodes, demonstrating significant potential for augmenting battery performance and prolonging their operational longevity.

4. Experimental section

The preparation method for MOF-74 coated Zn involves directly immersing polished and cleaned zinc foil into a methanol solution of 2,5-dihydroxyterephthalic acid (DHTA) and leaving it to stand. The standing times are 15 min. The concentration of the DHTA methanol solution is set at 2 g/L. After immersion, the zinc foil is removed and alternately washed with methanol and deionized water.

Supporting information

Experimental details of the controllable synthesis, physical characterization and electrochemical measurements.

CRediT authorship contribution statement

Da Bi: Writing – review & editing, Writing – original draft, Validation, Methodology, Investigation, Data curation. **Qingxue Lai:** Writing – review & editing, Methodology. **Tiantian Zhao:** Validation, Investigation, Conceptualization. **Sergey A. Grigoriev:** Validation. **Jingxiang Zhao:** Validation. **Yanyu Liang:** Writing – review & editing, Supervision.

Declaration of Competing Interest

The authors declare that they have no known competing financial interests or personal relationships that could have appeared to influence the work reported in this paper.

Data availability

Data will be made available on request.

Acknowledgements

This work was supported by the National Natural Science Foundation of China (Grant No. 21902077), the Natural Science Foundation of Jiangsu Province (BK20201287 and Grant No. BK20190381). We also gratefully acknowledge technical assistance from the Center for Microscopy and Analysis at Nanjing University of Aeronautics and Astronautics.

Appendix A. Supporting information

Supplementary data associated with this article can be found in the online version at doi:10.1016/j.jallcom.2024.175448.

References

[1] J.E. Trancik, Renewable energy: back the renewables boom, Nature 507 (2014) 300–302.
[2] H. Zhang, X. Liu, H. Li, I. Hasa, S. Passerini, Challenges and strategies for high-energy aqueous electrolyte rechargeable batteries, Angew. Chem. Int. Ed. 60 (2021) 598–616.
[3] B. Tang, L. Shan, S. Liang, J. Zhou, Issues and opportunities facing aqueous zinc-ion batteries, Energy Environ. Sci. 12 (2019) 3288–3304.
[4] M. Song, H. Tan, D. Chao, H.J. Fan, Recent advances in Zn-ion batteries, Adv. Funct. Mater. 28 (2018) 1802564.
[5] G. Fang, J. Zhou, A. Pan, S. Liang, Recent advances in aqueous zinc-ion batteries, ACS Energy Lett. 3 (2018) 2480–2501.
[6] Q. Yang, G. Liang, Y. Guo, Z. Liu, B. Yan, D. Wang, Z. Huang, X. Li, J. Fan, C. Zhi, Do zinc dendrites exist in neutral zinc batteries: a developed electrohealing strategy to in situ rescue in-service batteries, Adv. Mater. 31 (2019) 1903778.
[7] L. Suo, D. Oh, Y. Lin, Z. Zhuo, O. Borodin, T. Gao, F. Wang, A. Kushima, Z. Wang, H.-C. Kim, How solid-electrolyte interphase forms in aqueous electrolytes, J. Am. Chem. Soc. 139 (2017) 18670–18680.
[8] L.E. Blanc, D. Kundu, L.F. Nazar, Scientific challenges for the implementation of Zn-ion batteries, Joule 4 (2020) 771–799.
[9] Z. Cao, R. Ma, X. Xiao, D. Xiong, W. Yi, S. Tao, Z. Song, Y. Xiong, W. Deng, J. Hu, Single atom vacancy engineering with highly reversible N4 sites enable ultra-low overpotential for durable zinc-ion supercapacitors, Energy Storage Mater. 66 (2024) 103189.
[10] H. Jia, Z. Wang, B. Tawiah, Y. Wang, C.-Y. Chan, B. Fei, F. Pan, Recent advances in zinc anodes for high-performance aqueous Zn-ion batteries, Nano Energy 70 (2020) 104523.
[11] X. Pu, B. Jiang, X. Wang, W. Liu, L. Dong, F. Kang, C. Xu, High-performance aqueous zinc-ion batteries realized by MOF materials, Nano Micro Lett. 12 (2020) 1–15.
[12] P. Wang, S. Liang, C. Chen, X. Xie, J. Chen, Z. Liu, Y. Tang, B. Lu, J. Zhou, Spontaneous construction of nucleophilic carbonyl-containing interphase toward ultrastable zinc-metal anodes, Adv. Mater. 34 (2022) 2202733.
[13] F. Bu, Y. Gao, W. Zhao, Q. Cao, Y. Deng, J. Chen, J. Pu, J. Yang, Y. Wang, N. Yang, Bio-inspired trace hydroxyl-rich electrolyte additives for high-rate and stable Zn-ion batteries at low temperatures, Angew. Chem. 136 (2024) e202318496.
[14] Z. Xu, S. Jin, N. Zhang, W. Deng, M.H. Seo, X. Wang, Efficient Zn metal anode enabled by O, N-codoped carbon microflowers, Nano Lett. 22 (2022) 1350–1357.
[15] H. Wang, Y. Chen, H. Yu, W. Liu, G. Kuang, L. Mei, Z. Wu, W. Wei, X. Ji, B. Qu, A multifunctional artificial interphase with fluorine-doped amorphous carbon layer for ultra-stable Zn anode, Adv. Funct. Mater. 32 (2022) 2205600..
[16] C. Mao, Y. Chang, X. Zhao, X. Dong, Y. Geng, N. Zhang, L. Dai, X. Wu, L. Wang, Z. He, Functional carbon materials for high-performance Zn metal anodes, J. Energy Chem. 75 (2022) 135–153.
[17] Z. Cai, Y. Ou, J. Wang, R. Xiao, L. Fu, Z. Yuan, R. Zhan, Y. Sun, Chemically resistant Cu–Zn/Zn composite anode for long cycling aqueous batteries, Energy Storage Mater. 27 (2020) 205–211.
[18] Q. Zhang, J. Luan, L. Fu, S. Wu, Y. Tang, X. Ji, H. Wang, The three-dimensional dendrite-free zinc anode on a copper mesh with a zinc-oriented polyacrylamide electrolyte additive, Angew. Chem. Int. Ed. 58 (2019) 15841–15847.
[19] G. Liang, J. Zhu, B. Yan, Q. Li, A. Chen, Z. Chen, X. Wang, B. Xiong, J. Fan, J. Xu, Gradient fluorinated alloy to enable highly reversible Zn-metal anode chemistry, Energy Environ. Sci. 15 (2022) 1086–1096.
[20] M. Zhu, J. Hu, Q. Lu, H. Dong, D.D. Karnaushenko, C. Becker, D. Karnaushenko, Y. Li, H. Tang, Z. Qu, A patternable and in situ formed polymeric zinc blanket for a reversible zinc anode in a skin-mountable microbattery, Adv. Mater. 33 (2021) 2007497.
[21] H. Yang, Z. Chang, Y. Qiao, H. Deng, X. Mu, P. He, H. Zhou, Constructing a super-saturated electrolyte front surface for stable rechargeable aqueous zinc batteries, Angew. Chem. 132 (2020) 9463–9467.
[22] R. Yuksel, O. Buyukcakir, W.K. Seong, R.S. Ruoff, Metal-organic framework integrated anodes for aqueous zinc-ion batteries, Adv. Energy Mater. 10 (2020) 1904215.
[23] C. Wang, J. Kim, J. Tang, M. Kim, H. Lim, V. Malgras, J. You, Q. Xu, J. Li, Y. Yamauchi, New strategies for novel MOF-derived carbon materials based on nanoarchitectures, Chem 6 (2020) 19–40.
[24] Z. Wang, L. Dong, W. Huang, H. Jia, Q. Zhao, Y. Wang, B. Fei, F. Pan, Simultaneously regulating uniform Zn 2+ flux and electron conduction by MOF/rGO interlayers for high-performance Zn anodes, Nano Micro Lett. 13 (2021) 1–11.
[25] Z. Cao, H. Zhang, B. Song, D. Xiong, S. Tao, W. Deng, J. Hu, H. Hou, G. Zou, X. Ji, Angstrom-level ionic sieve 2D-MOF membrane for high power aqueous zinc anode, Adv. Funct. Mater. 33 (2023) 2300339.
[26] Y. Xiang, Y. Zhong, P. Tan, L. Zhou, G. Yin, H. Pan, X. Li, Y. Jiang, M. Xu, X. Zhang, Thickness-controlled synthesis of compact and uniform MOF protective layer for zinc anode to achieve 85% zinc utilization, Small 19 (2023) 2302161.
[27] Y. Wang, Y. Liu, H. Wang, S. Dou, W. Gan, L. Ci, Y. Huang, Q. Yuan, MOF-based ionic sieve interphase for regulated Zn 2+ flux toward dendrite-free aqueous zinc-ion batteries, J. Mater. Chem. A 10 (2022) 4366–4375.
[28] S. Lawson, A. Siemers, J. Kostlenick, Q. Al-Naddaf, K. Newport, A.A. Rownaghi, F. Rezaei, Mixing Mg-MOF-74 with Zn-MOF-74: a facile pathway of controlling the pharmacokinetic release rate of curcumin, ACS Appl. Biol. Mater. 4 (2021) 6874–6880.
[29] T.G. Glover, G.W. Peterson, B.J. Schindler, D. Britt, O. Yaghi, MOF-74 building unit has a direct impact on toxic gas adsorption, Chem. Eng. Sci. 66 (2011) 163–170.
[30] Z. Gao, Y. Lai, L. Zhang, Y. Lin, L. Xiao, Y. Luo, F. Luo, Synthesis, characterization, and electrocatalytic activity exploration of MOF-74: a research-style laboratory experiment, J. Chem. Educ. 98 (2021) 3341–3347.
[31] A. Vimont, J.-M. Goupil, J.-C. Lavalley, M. Daturi, S. Surblé, C. Serre, F. Millange, G. Férey, N. Audebrand, Investigation of acid sites in a zeotypic giant pores chromium (III) carboxylate, J. Am. Chem. Soc. 128 (2006) 3218–3227.
[32] E. Ozyilmaz, O. Caglar, Rapid mechanochemical production of biocomposites by encapsulating enzymes to zinc based-two metal organic frameworks (ZIF-8 and Zn-MOF-74) for enantioselective hydrolysis reaction of racemic Naproxen methyl ester, Process Biochem. 134 (2023) 276–285.
[33] L. Zhang, L. Miao, W. Xin, H. Peng, Z. Yan, Z. Zhu, Engineering zincophilic sites on Zn surface via plant extract additives for dendrite-free Zn anode, Energy Storage Mater. 44 (2022) 408–415.
[34] D. Wang, Q. Li, Y. Zhao, H. Hong, H. Li, Z. Huang, G. Liang, Q. Yang, C. Zhi, Insight on organic molecules in aqueous Zn-ion batteries with an emphasis on the Zn anode regulation, Adv. Energy Mater. 12 (2022) 2102707.
[35] M. Zhou, S. Guo, J. Li, X. Luo, Z. Liu, T. Zhang, X. Cao, M. Long, B. Lu, A. Pan, Surface-preferred crystal plane for a stable and reversible zinc anode, Adv. Mater. 33 (2021) 2100187.
[36] L. Sha, B.-B. Sui, P.-F. Wang, Z. Gong, Y.-H. Zhang, Y.-H. Wu, L.-N. Zhao, J.-J. Tang, F.-N. Shi, 3D network of zinc powder woven into fibre filaments for dendrite-free zinc battery anodes, Chem. Eng. J. 481 (2024) 148393.
[37] B.-b Sui, L. Sha, P.-f Wang, Z. Gong, Y.-h Zhang, Y.-h Wu, L.-n Zhao, J.-j Tang, F.-n Shi, In situ zinc citrate on the surface of Zn anode improves the performance of aqueous zinc-ion batteries, J. Energy Storage 82 (2024) 110550.
[38] B.-b Sui, L. Sha, Q.-p Bao, P.-f Wang, Z. Gong, M.-d Zhou, F.-n Shi, K. Zhu, Polyoxometalate solution passivation enabling dendrite-free and high-performance zinc anodes in aqueous zinc-ion batteries, J. Colloid Interface Sci. 669 (2024) 886–895.
[39] L. Yao, C. Hou, M. Liu, H. Chen, Q. Zhao, Y. Zhao, Y. Wang, L. Liu, Z.W. Yin, J. Qiu, Ultra-stable Zn anode enabled by fiber-directed ion migration using mass-producible separator, Adv. Funct. Mater. 33 (2023) 2209301.
[40] J. Zhang, P. Li, Y. Wang, Z. Zhao, Z. Peng, Linking interfacial hydrogen-bond network to electrochemical performance of zinc anode in aqueous solution, Adv. Funct. Mater. 33 (2023) 2305804.

[41] R. Wang, Q. Ma, L. Zhang, Z. Liu, J. Wan, J. Mao, H. Li, S. Zhang, J. Hao, L. Zhang, An aqueous electrolyte regulator for highly stable zinc anode under− 35 to 65° C, Adv. Energy Mater. 13 (2023) 2302543.
[42] J. Zhou, L. Zhang, M. Peng, X. Zhou, Y. Cao, J. Liu, X. Shen, C. Yan, T. Qian, Diminishing interfacial turbulence by colloid-polymer electrolyte to stabilize zinc ion flux for deep-cycling Zn metal batteries, Adv. Mater. 34 (2022) 2200131.
[43] W.W. Rudolph, M.H. Brooker, P. Tremaine, Raman-and infrared spectroscopic investigation of aqueous ZnSO4 solutions from 8C to 165C: inner-and outer-sphere complexes, Z. F. üR. Phys. Chem. 209 (1999) 181–207.
[44] T. Wang, Q. Xi, Y. Li, H. Fu, Y. Hua, E.G. Shankar, A.K. Kakarla, J.S. Yu, Regulating dendrite-free zinc deposition by red phosphorous-derived artificial protective layer for zinc metal batteries, Adv. Sci. 9 (2022) 2200155.
[45] T.C. Li, D. Fang, J. Zhang, M.E. Pam, Z.Y. Leong, J. Yu, X.L. Li, D. Yan, H.Y. Yang, Recent progress in aqueous zinc-ion batteries: a deep insight into zinc metal anodes, J. Mater. Chem. A 9 (2021) 6013–6028.
[46] F. Wang, J. Tseng, Z. Liu, P. Zhang, G. Wang, G. Chen, W. Wu, M. Yu, Y. Wu, X. Feng, A stimulus-responsive zinc–iodine battery with smart overcharge self-protection function, Adv. Mater. 32 (2020) 2000287.
[47] Y. Mao, Z. Li, Y. Li, D. Cao, G. Wang, K. Zhu, G. Chen, Breaking intramolecular hydrogen bonds of polymer films to enable dendrite-free and hydrogen-suppressed zinc metal anode, Chem. Eng. J. 461 (2023) 141707.